Accuracy Limits of step response Dynamics on Laser-Induced Forward Transfer of a Near-Infrared Nanosecond-Pulse Laser on Thin Gold Films

S.T.C. Fokkema*,[1], M. Feinaeugle[1]

*corresponding author s.t.c.fokkema@student.utwente.nl
[1]Chair of Laser Processing, Department of Mechanics of Solids, Surfaces and Systems (MS3), Faculty of Engineering Technology (ET), University of Twente, Drienerlolaan 5, 7522 NB, Enschede, The Netherlands

ABSTRACT: The accuracy of Laser-induced forward transfer (LIFT) with a moving donor and receiver was examined, A nanosecond-pulse laser with a 1064 nm central wavelength onto a 400 nm thick film of gold (Au) was used as a setup. Droplet ejection was well predicted by existing literature on nanosecond LIFT of gold though ablation spots were found on the receiver. No dependence of the donor morphology on the repetition rate was observed. A linear dependence of the deposition deflection on the donor velocity and donor acceleration were found with the deviation still being dominant and within expectations. A step response assembly-scheme was created and analysed. For preserving acceptable deposit accuracy. Constraints on the four mechanical parameters were established. These findings show the viability of the LIFT setup made and establish constraints on LIFT scalability using a step response scheme and for adjusting a system with a changing equivalent mass.

Key words: Laser-Induced Forward Transfer, Accuracy, Gold, Dynamics, Nanosecond-Pulse, step response

1 INTRODUCTION

3D printing is a recently created group of manufacturing methods that allows manufacturing from a pre-recorded digital input file. It is a rapidly growing technique for many different kinds of materials. [1]
For metals, there is a large interest in depositing small structures because of the widespread use of this class of materials, for example, in electronics.
Direct writing methods, which allow the printing of material from a pattern one voxel at a time, are well suited to meet this upcoming digital demand [2]. Examples of current widespread direct-writing methods are inkjet printing and aerosol printing. However, these techniques have constraints on the rheology of processable inks and on the printable resolution [3].

Laser-induced forward transfer, LIFT, is a direct-writing technique involving a pulsed laser to propel a volume of material onto a surface. LIFT was first termed in 1986 when Bohandy et al. [4] successfully deposited copper (Cu) using an examiner laser. Figure 1 [3] visually shows the LIFT process.

In the classical and most common LIFT configuration, a pulsed laser is focused at the intersection of a transparent plate (`carrier`) and a thin film (`donor`). As a result, material is transferred from the donor. A surface plane (`receiver`) parallel to the carrier substrate separated a few microns from the donor collects the transferred material. With metal donors, the radiative energy of the laser pulse is absorbed in the donor; This leads to rapid melting and partial vaporization of a well-defined volume of the donor resulting in a drop-based ejection towards the receiver [3].

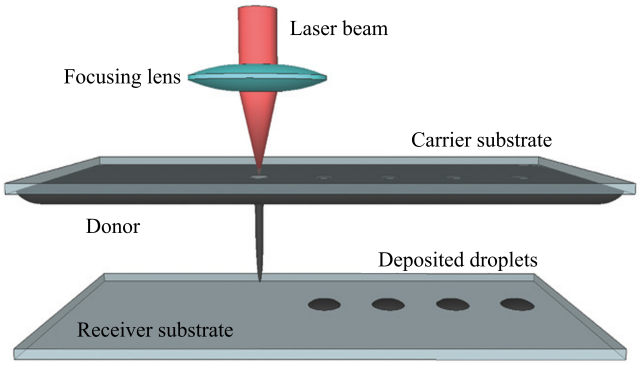

Figure 1: Laser-induced forward transfer. Adapted from: [3]

Droplet-based LIFT of metals is gaining traction as a microfabrication method due to the high degree of control of droplet formation, the easy implementation and the competitive resolution (sub-100 nm to μm) compared to other additive manufacturing methods [5] and is now being explored for the microfabrication of, for example, metal circuits [6], vias [7], photonic structures [8] and microscale 3D printing [9].
Previously, Feinaeugle et al. [10] used a sacrificial approach combining LIFT and chemical etching to make complex free-standing metallic microstructures with a pulse rate (`repetition rate`) of 1.5 Hz.
However, to create better microfabrication scalability, higher printing speeds (donor speed, donor acceleration, repetition rate) should be closely examined [11].

For this paper, a setup of classical LIFT was made and focused with a nanosecond laser with a central wavelength of 1064 nm onto a 400 nm thick gold film:

1. The morphologies of the donor and the receiver substrate were examined to analyse the nature of the material transfer mechanism.
2. The threshold fluence was measured and compared with existing literature on nanosecond LIFT of metals for smaller central wavelengths.
3. The dependence of the deposition position on the donor-receiver speed (`speed`) was examined within the range of 20 mm/s to 52 mm/s.
4. The dependence of the deposition position on the donor-receiver acceleration (`acceleration`) was examined within the range of -1.97 m/s^2 to 1.97 m/s^2.
5. The dependence of the donor surface morphology on the repetition rate was examined within the range of 1 kHz to 10 kHz.
6. A theoretical scheme of applying multiple step-inputs (`assembly`) was created and examined.
7. The speed and acceleration of this step response scheme were compared with the results of the deposition position measurements to examine constraints on the four mechanical parameters (m, d, k, h) of a system.

2 THEORETICAL

2.1 Ejection Mechanism

The laser pulse duration spent at or above $1/e$ of its maximum power is termed the laser `pulse width`. For LIFT with a pulse width on the order of nanoseconds and using metallic donors, Figure 2 [3] breaks down the transfer mechanism into four phases:

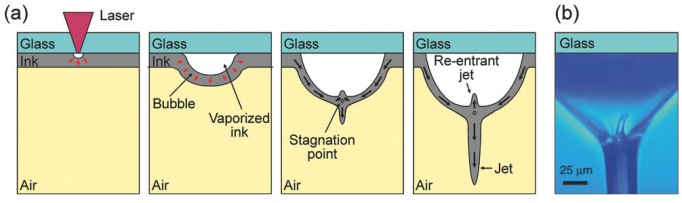

Figure 2: Deposition mechanism of liquid LIFT of metals. Four phases exist: (1) the laser pulse heats the interface of the film at the donor substrate; (2) a resulting melt front propagates through the film until it reaches the free surface; (3) at about this time, the material at the interface is superheated beyond its boiling point until; (4) the resulting vapour-induced pressure at the interface propels the molten film forward towards the receiver. [3]

The total radiative energy per unit area of a laser pulse (`fluence`) on the donor surface has a strong effect on the transfer (`deposition`) mechanism that occurs. Wu et al. [12] found two threshold fluences for nanosecond LIFT of metals, creating three ejection regimes: The non-release regime, the single droplet regime and the splash regime for increasing fluences. Schultze and Wagner [13,14] found two more deposition modes for nanosecond LIFT of metals. Transfer of thin donor films and/or moderate fluences results in deposits smaller than the laser spot size. Transfer of thick donor films and/or large fluences results in deposits larger than or close to the laser spot size.

2.2 Threshold laser fluence

The `thermal diffusion length`, L_{th}, is a measure of the rate at wich heat propagates through a material and is another important parameter for determining the nature of transfer. It was estimated with $L_{\mathrm{th}} = 2\sqrt{\alpha\tau_{\mathrm{p}}}$ [5] where $\tau_{\mathrm{p}} = 50$ ns is the laser pulse width [15] and $\alpha = 1.27$ cm^2/s [16] is the thermal diffusivity of solid gold (Au), giving $L_{\mathrm{th}} = 5.04$ µm. This is an order of magnitude above the film thickness, making the film near-isothermal throughout its thickness [17]. This means that a full-thickness cylinder with the laser spot size as the diameter needs to be superheated to its boiling point. Equation (1) then estimates the threshold fluence, φ_{Au} [18]:

$$\varphi_{\mathrm{Au}} = D\frac{C_{p,\mathrm{s}}T_{\mathrm{s}} + C_{p,\mathrm{l}}T_{\mathrm{l}} + \rho(L_{\mathrm{m}} + L_{\mathrm{v}})}{1 - R} \quad [\mathrm{J/m^2}] \quad (1)$$

where $T_{\mathrm{s}} = 1064$ K and $T_{\mathrm{l}} = 1766$ K are the temperature rises in the solid phase and liquid phase respectively, $C_{p,\mathrm{s}} = 2.48$ MJ/(m^{3}K) and $C_{p,\mathrm{l}} = 2.90$ MJ/(m^{3}K) [19] are the heat capacities of solid gold and liquid gold respectively, $L_{\mathrm{m}} = 64.5$ kJ/kg and $L_{\mathrm{v}} = 1645$ kJ/kg are the latent heat of melting and the latent heat of vaporization of gold respectively, $D = 400$ nm is the donor film thickness, $\rho = 19.3 \cdot 10^3$ kg/m^3 is the mass density of solid gold and $R = 0.99$ is the optical reflectance for a semi-infinitely thick plate of solid gold [20]. Equation (1) then gives a threshold laser fluence of $\varphi_{\mathrm{Au}} = 163.01$ J/cm^2. [18]

2.3 Ejection Trajectory

Besides just the threshold fluences, the ejection trajectory is also heavily dependent on process parameters and, in particular, the distance between the donor and the receiver (`gap spacing`), Δz.

Pohl et al. [18] achieved nanosecond LIFT with a 200 nm gold film and observed deposition at ~ 10 m/s at a deflected angle $0° \leq \theta \leq 42.5°$ with the vertical in the radial direction, giving a spread in deposition.
Sano et al. [21] performed nanosecond LIFT on gold films and observed a dependence of the deposition spread on the laser fluence. Higher laser fluences increased the deposition angle, θ.

2.4 Receiver Substrate Ablation

At very high laser fluences, material can also be removed directly from a surface (`ablation`) when exposed to fluence above the ablation threshold fluence. Rastogi et al. [22] examined ablation of BK7 glass, the receiver substrate material, for a 9 ns pulse laser with a central wavelength of 1064 nm. An ablation threshold laser fluence, φ_{BK7}, of 75 J/cm^2 was found. Chen et al. [23] found a power relation $\varphi_{\mathrm{BK7}} \propto \tau_{\mathrm{p}}^{\vartheta}$ of the threshold laser fluence of BK7 glass with the laser pulse width, τ_{p}, where $0.3 < \vartheta < 0.6$. For $\tau_{\mathrm{p}} = 50$ ns, this results in 125 J/cm^2 $< \varphi_{\mathrm{BK7}} < 209$ J/cm^2.

3 EXPERIMENTAL

3.1 Experimental Setup

Figure 3 schematically shows the experimental setup that was made by the author.
In the setup, pulses with a laser pulse width of 50 ns for a laser source (redENERGY G4Z A1, SPI) operating at a central wavelength of 1064 nm with a Gaussian spatial profile ($M^2 \leq 1.6$), were focused onto the interface of a borosilicate glass carrier and the donor. The donor is a sputtered 400 nm thick gold film.
A 25.6 mm plano-convex lens (LA1229-C, Thorlabs) was mounted - along with two dielectric mirrors (BB1-E03P, Thorlabs) - onto a linear translation stage (ATS100-100-BRK, Aerotech) to adjust the focus distance in the vertical (z) direction.
The carrier-donor and receiver laid in near-contact. Focusing with an optical microscope measured a gap spacing of $\Delta z < 43$ µm between the two surfaces.
The carrier-donor-receiver assembly was mounted onto a Cartesian set (x, y) of linear translational stages (ALS130-150-LTAS-25DU-NC, Aerotech).
Gold was chosen for its compliance with LIFT setups due to its resistance to oxidation, good temperature stability, and low loss in the near-infrared (NIR) range [24], along with good process documentation and relevance to microelectronic development.

3.2 Measuring Equipment

The correct focus distance for a wavelength of 1064 nm was obtained by irradiating a metal coin on the receiver mount at a continuous range of focus distances. The setting that gave the largest features on the coin was converted into the equivalent setting for LIFT[1].
The mean pulse energy was measured using a multimeter (FieldMaxII-TO, Coherent) combined with a laser power sensor (PowerMax-USB PM10, Coherent) positioned in the path of the laser between the focusing lens and the carrier substrate.
Morphologies of the donor surface and the receiver deposits were examined using optical microscopy and dark field microscopy (DMRM, Leica Leitz).

3.3 Pulse Energy Measurements

With a repetition rate of 1 kHz, a sequential series of pulses was irradiated for a variety of mean pulse energies in a range of 36.5 µJ to 73.5 µJ. During periodical irradiation, the (y)-stage was moved in a straight line at a speed of 20 mm/s to ensure that the craters in the donor were spaced and did not interact.

3.4 Repetition Rate Measurements

With a mean pulse energy of 42.5 µJ, a sequential series of pulses was irradiated for a variety of repetition rates, r, in a range of 1 kHz to 10 kHz. During periodical irradiation, the (y)-stage was moved in a straight line at a speed of $r \cdot 10$ µm.

3.5 Deposit Position Measurements

With a repetition rate of 1 kHz and a mean pulse energy of 42.5 µJ, a sequential series of pulses was irradiated. During periodical irradiation, the (x, y)-stages made two different sine-wave movements.
One with a translation speed of 20 mm/s with a 10 Hz transverse oscillation at an amplitude of 0.5 mm, and another with a translation speed of 40 mm/s with a 10 Hz transverse oscillation at an amplitude of 0.5 mm, to ensure that the craters in the donor were spaced and did not interact. This varied movement through a range of speeds and accelerations from 20 mm/s to 52 mm/s and -1.97 m/s^2 to 1.97 m/s^2 respectively.

[1] Refraction in the carrier substrate was considered using Snell's law of refraction [25]. The index of refraction was found using the Sellmeier equation [26]. The beam radius entering the plano-convex lens was found using a continually adjustable pinhole. The optimal laser spot size, $2\omega_0$, was also computed.

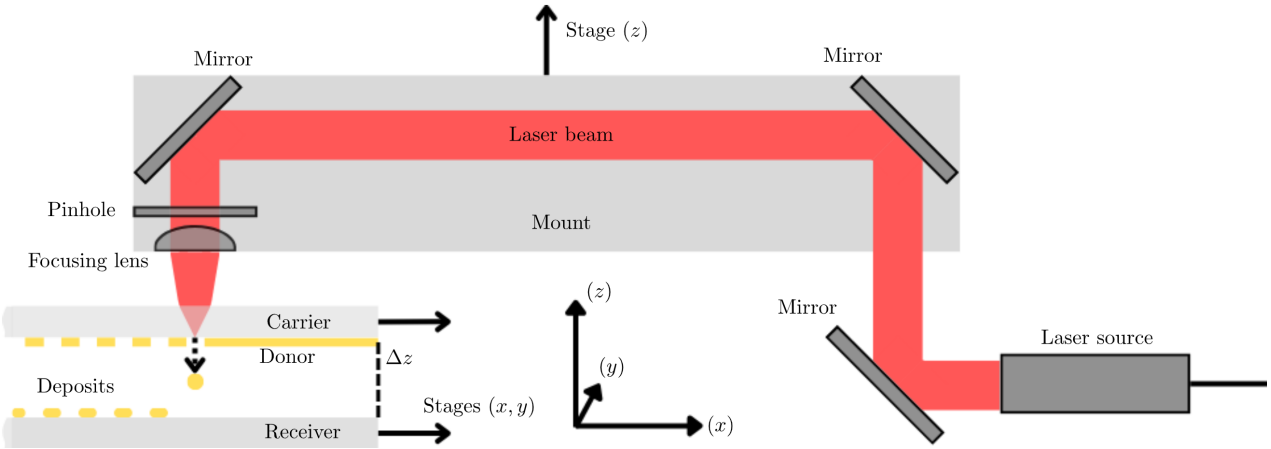

Figure 3: Schematic of the experimental LIFT setup that was made and used for the experiments. Dimensions are not to scale.

4 RESULTS

4.1 Pulse Energy Measurements

Figure 4 shows the donor-carrier interface surface:

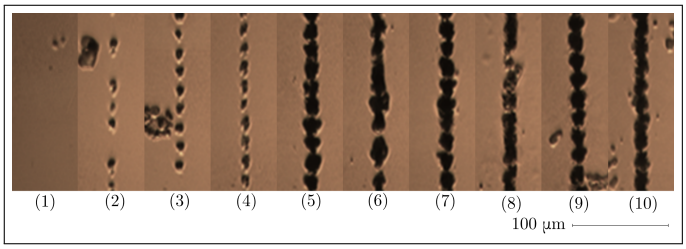

Figure 4: Optical top-view of the donor-carrier interface surface at (1) 36.5 µJ, (2) 38.4 µJ, (3) 42.5 µJ, (4) 44.5 µJ, (5) 49.7 µJ, (6) 53.1 µJ, (7) 64.2 µJ, (8) 65.3 µJ, (9) 70.1 µJ, (10) 73.5 µJ.

Figure 4 shows that above the mean pulse energy threshold of 42.5 µJ, the donor morphology changes from irregular "markings" to the creation of a "black" hole. Thus, 42.5 µJ is the pulse energy threshold.
Figure 5 shows a single donor crater at this mean pulse energy and shows two distinct features;

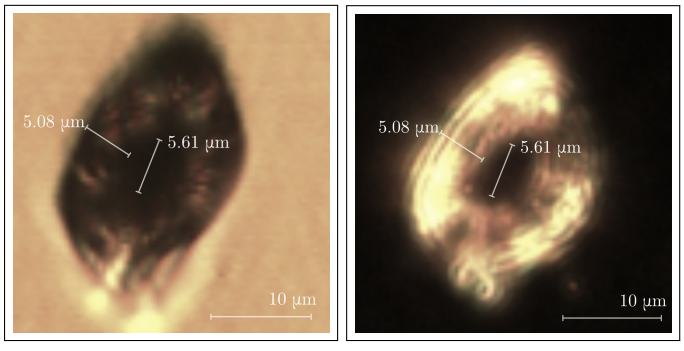

Figure 5: Top-view of the donor-carrier interface surface crater at 42.5 µJ with (a) optical microscopy, (b) dark field microscopy.

The first feature is a "centre circle" of removed material. This is surrounded by the second feature, a "ring" of ablated or deformed material.
With a transmissivity of the carrier substrate (borosilicate glass) of 0.945 [26] and a spot size of 5.61 µm, a threshold laser fluence of 162.48 J/cm^2 is found.
Table 1 summarises the predicted parameters versus the measured parameters. It shows that the thickness of this "ring" lines up with the computed thermal diffusion length and the "inner circle" diameter is within $\sqrt{2}$ of the computed optimal spot size, and the laser threshold fluence lines up with the predicted value:

Table 1: Predicted parameters versus measured parameters.

Term	**Predicted**	**Measured**	**Difference**
L_{th}	5.03 µm	5.08 µm	(+)0.99%
$2\omega_0$	4.4 µm	5.61 µm	(+)27.5%
φ_{Au}	163.01 J/cm^2	162.48 J/cm^2	(−)0.3%

4.2 Repetition Rate Measurements

Figure 6 shows the donor-carrier interface surface:

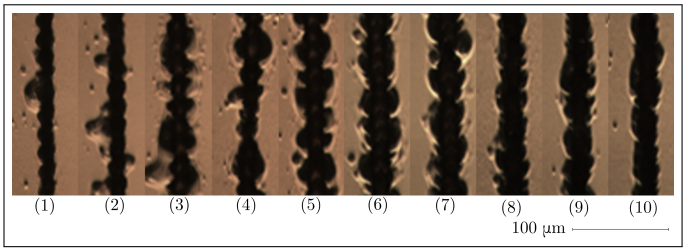

Figure 6: Optical top-view of the donor-carrier interface surface at 42.5 µJ with (1) 1 kHz, (2) 2 kHz, (3) 3 kHz, (4) 4 kHz, (5) 5 kHz, (6) 6 kHz, (7) 7 kHz, (8) 8 kHz, (9) 9 kHz, (10) 10 kHz.

Figure 6 shows that there were no significant differences in donor morphology.

4.3 Deposit Position Measurements

4.3.a Qualitative

Figure 7 shows the receiver substrate surface and shows five different observations:

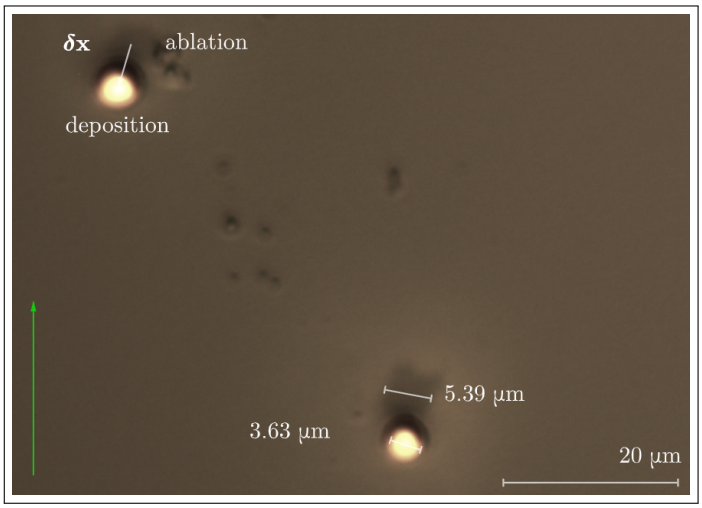

Figure 7: Optical top-view of the receiver substrate surface.

These observations consist of the following:

- The brightly coloured discs are the deposited gold droplets. Deposited single droplets were observed to have a diameter of $\sim$ 3.69 µm. Few satellite droplets were observed near of this droplet, meaning that all donor crater volume was transferred into a single droplet regime.
- The droplet was observed to be smaller in diameter than the crater size on the donor-carrier interface surface, supporting the occurrence of LIFT in the thin film regime; Full melt propagation then occurred during ejection [13, 14].
- Another sequential set of discolourations is observed on the receiver. These were ablation spots of the receiver substrate material. This means that the laser through transmission of the gold film, before ejection occurs, exceeded the ablation threshold laser fluence of the receiver.
- The diameter of the ablation spot, 5.39 µm, closely matched the found spot size ((+)3.9%).
- The volume of a half-sphere with 3.69 µm had the same volume as a cylinder with a length of 400 nm ((+)0.6%) and a diameter of 5.61 µm. Assuming an equal mass density between both volumes with the mass density of solid gold at room temperature, this means that the deposited droplets had a half-spherical profile, and ejection in the single-droplet regime occurred.
- The difference in location of the deposited droplets and the ablation spots (irradiation position) shows droplets underwent a `translation`, $\mathbf{\delta x}$, with respect to the receiver and donor.

4.3.b Quantitative

The difference between the ablation spot position and the droplet position gave the droplet translation[2].
The involved nonlinear effects to the droplet translation cannot generally be decomposed via superposition. Equation (2) therefore consciously splits the droplet translations into two components[3]: the component, $\delta x_{\hat{\mathbf{v}}}$, of the velocity, $\hat{\mathbf{v}}$, and the component, $\delta x_{\hat{\mathbf{a}}}$, of the acceleration, $\hat{\mathbf{a}}$:

$$\mathbf{\delta x} = \delta x_{\hat{\mathbf{v}}}\hat{\mathbf{v}} + \delta x_{\hat{\mathbf{a}}}\hat{\mathbf{a}} \qquad \text{[m]} \quad (2)$$

Figure 8 shows the droplet translation component of the velocity plotted against the speed:

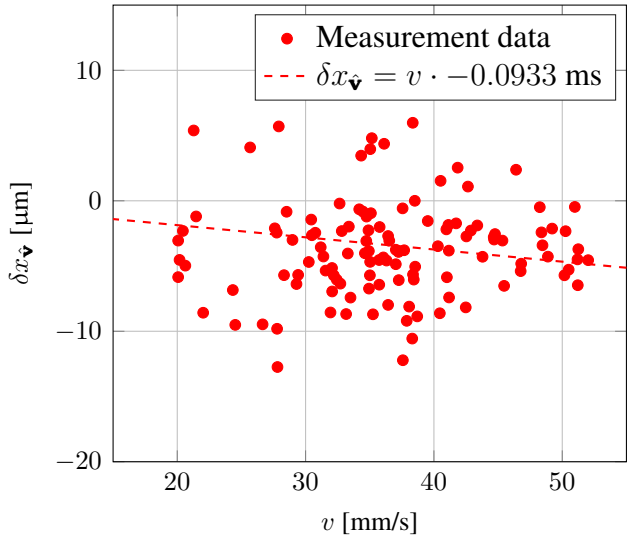

Figure 8: The translation component, $\delta x_{\hat{\mathbf{v}}}$, of the velocity versus the speed, v. A dependence of $\delta x_{\hat{\mathbf{v}}} = v \cdot -0.0933$ ms was computed with a squared correlation coefficient of $R^2 = 0.4412$.

The trend in Figure 8 shows that at a speed of $v_{\max} = 39.54$ mm/s, the droplet translation component exceeds the droplet diameter and becomes undesirable. Figure 9 shows the droplet translation component of the acceleration plotted against the acceleration, and the trend shows that until an acceleration of $|a_{\max}| = 1.97$ mm/s^2, the droplet translation component is below the droplet diameter and remains desirable.

[2]The translations of droplets with a diameter above 4 µm were plotted. Some depositions occurred in the splash regime. These depositions were neglected in this analysis.

[3]The basis $(\hat{\mathbf{v}}, \hat{\mathbf{a}})$ is generally not orthonormal. This makes splitting the translation into two components more delicate.

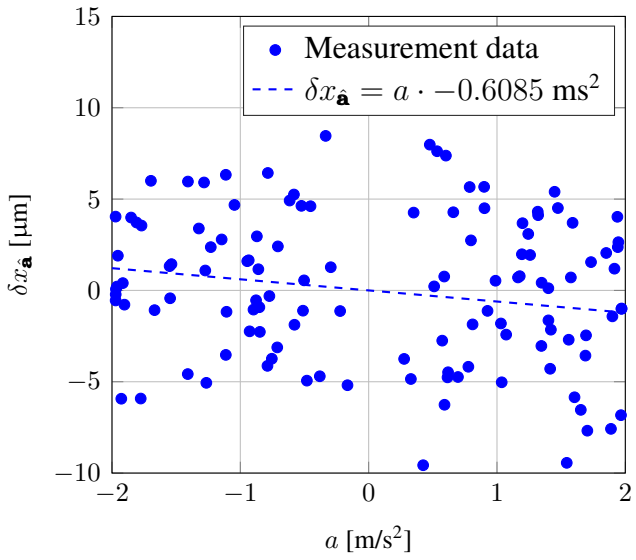

Figure 9: The droplet translation component, $\delta x_{\hat{\mathbf{a}}}$, of the acceleration versus the acceleration, a. A dependence of $\delta x_{\hat{\mathbf{a}}} = a \cdot -0.6085$ ms^2 was computed with a squared correlation coefficient of $R^2 = 0.0333$.

Both graphs also show deviation in components in a continuous range of a size below $\Delta z\sqrt{2}\cos(42.5°) = 43.7$ µm, which agrees with existing literature [18]. Table 2 shows a statistical analysis for both relations and shows that they are both statistically significant:

Table 2: The z-value, z_R, or a random/coincidental distribution, a Gaussian distribution with $\mu_R = 0$, $\sigma_R = 1/\sqrt{n}$, assumed for R is computed for the obtained R. n is the measurement count.

Relation	$\boldsymbol{R}$	$\boldsymbol{\sigma_R}$	$\boldsymbol{z_R}$
$\delta x_{\hat{\mathbf{v}}} = v \cdot -0.0933$ ms	0.6642	0.0913	7.2763
$\delta x_{\hat{\mathbf{a}}} = a \cdot -0.6085$ ms^2	0.1825	0.0913	1.9990

5 DISCUSSION

5.1 *The Step Response*

The linear second-order step response of a time-invariant single-input-single-output (SISO) system was examined[4]. In the time-domain, t, Equation (3) shows the constraints on the deflection, $u(t)$, captured by a time-invariant differential equation [27]:

$$m\ddot{u}(t) + d\dot{u}(t) + ku(t) = F(t) \qquad [\text{kgm/s}^2] \quad (3)$$

where m is the equivalent mass, d is the equivalent damping factor, k is the equivalent stiffness and $F(t)$ is the equivalent external load on the system.

[4]For flexure-based systems and systems using LIM's, this is a valid assumption for small deflection magnitudes.

The initial conditions of $u(0) = 0$ m/s and $\dot{u}(0) = 0$ m/s^2 were used. A step-input was used, which means $F(t) = hH(t)$ where h is the equivalent input and $H(\cdot)$ is the Heavyside step-function.
Equation (4) gives the general solution[5] to this differential equation for the given external load and initial conditions, the step response, $u_h(t)$, for $t \geq 0$ [28]:

$$u_h(t) = S - S\frac{\omega_\text{n}}{\omega_\text{d}} e^{-\zeta\omega_\text{n}t}\sin(\omega_\text{d}t - \beta) \qquad [\text{m}] \quad (4)$$

where $\omega_n \equiv \sqrt{k/m}$ is the angular natural frequency, $\zeta \equiv d/(2\omega_\text{n}m)$ is the relative damping, $\omega_\text{d} \equiv \omega_\text{n}\sqrt{1-\zeta^2}$ is the angular damped natural frequency and $\beta \equiv \arcsin\zeta$ is the phase shift. $S \equiv h/k$ is the step size, which maximally equals the droplet diameter of 3.69 µm.
The response reaches the intended step at the rise time, $t_\text{r} \equiv (\pi/2 + \beta)/\omega_\text{d}$, and will maximally overshoot at the peak time, $t_\text{p} \equiv \pi/\omega_\text{d}$, before undergoing a damping oscillation at an angular frequency of ω_d.

5.2 *Assembly of Multiple Step Responses*

Equation (5) `assembles` j step-inputs. The deflection can be computed with Equation (4) and linear superposition analogous to a discrete convolution.

$$F(t) = h\sum_{i=0}^{j-1} H(t - t_\text{p}i) \qquad [\text{kgm/s}^2] \quad (5)$$

It was noticed that $u_h(t_r + t_p i) = h$ for all $i \in \mathbb{N}$ always holds and at t_p the response always equals the initial velocity. Thus, the movement path becomes: engage the next step-input at t_p and eject a droplet at t_r after engaging the new step input.
This step response assembly can be used to achieve `equally spaced ejections` of droplets.
However, Equations (6),(7) show a nonzero velocity and acceleration are present at $t_\text{r} + t_\text{p}i$ for all $i \in \mathbb{N}$:

$$\dot{u}_h(t_\text{r} + t_\text{p}i) = (-1)^i S\omega_\text{n}e^{-\zeta\omega_\text{n}(t_\text{r}+t_\text{p}i)} \qquad [\text{m/s}] \quad (6)$$

$$\ddot{u}_h(t_\text{r} + t_\text{p}i) = (-1)^i S\omega_\text{n}^2\zeta e^{-\zeta\omega_\text{n}(t_\text{r}+t_\text{p}i)} \qquad [\text{m/s}^2] \quad (7)$$

It can be shown that, using a finite summation of a geometric sequence, the total velocity and acceleration at ejection of this assembly of step responses have a strictly smaller magnitude than would result from a single step response. Therefore, the obtained velocity and acceleration limits are merely applied to the "worst-case" scenario of a single step response at t_r. This logically means $v = \dot{u}_h(t_\text{r})$ and $|a| = \ddot{u}_h(t_\text{r})$.

[5]An underdamped system ($0 < \zeta < 1$) was taken.

5.3 *Constraints on the four Mechanical Parameters*

Equation (8) defines the printing speed, V:

$$V \equiv \frac{S}{t_\mathrm{p}} = \frac{S\omega_\mathrm{d}}{\pi} = \frac{S\omega_\mathrm{n}}{\pi}\sqrt{1-\zeta^2} \qquad \text{[m/s]} \quad (8)$$

$\dot{u}_h(t_\mathrm{r})$ equals $S\omega_\mathrm{n}$ times a dimensionless function, $f(\zeta)$. $\ddot{u}_h(t_\mathrm{r})$ equals $S\omega_\mathrm{n}^2$ times a dimensionless function, $g(\zeta)$. Equations (9),(10) alternatively give V by substituting Equation (8) for ω_n and solving for V:

$$V_\mathrm{v}(\zeta, v) = \frac{v\sqrt{1-\zeta^2}}{\pi f(\zeta)} \qquad \text{[m/s]} \quad (9)$$

$$V_\mathrm{a}(\zeta, a) = \sqrt{\frac{S|a|\,(1-\zeta^2)}{\pi^2 g(\zeta)}} \qquad \text{[m/s]} \quad (10)$$

Figure 10 plots both functions at: v_max and a_max:

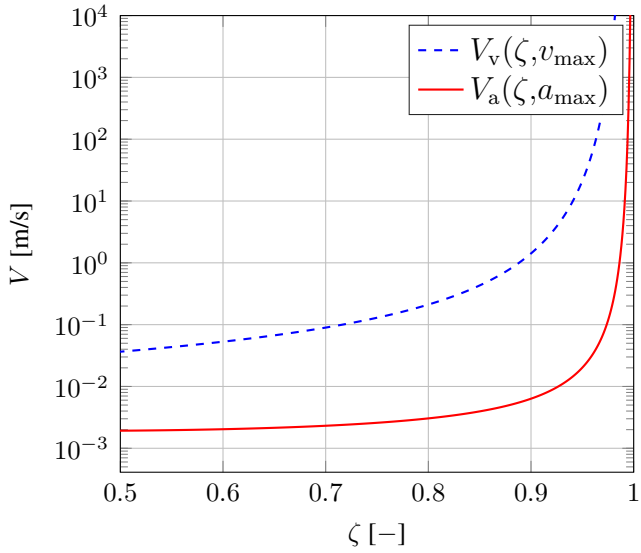

Figure 10: Logarithmic plot of $V_\mathrm{v}(\zeta, v_\mathrm{max})$ and $V_\mathrm{a}(\zeta, a_\mathrm{max})$.

Because the droplet translation components are proportional to v and a respectively, droplet translation is acceptable if the state (ζ, V) is below both curves. Thus, a valid couple of ζ and V can be manually chosen from this graph. Equations (11),(12),(13) then gives the constraints on the four mechanical parameters (m, d, k, h) for the chosen couple of ζ and V:

$$k = \frac{\pi^2 V^2}{S^2\,(1-\zeta^2)}m \qquad \text{[kg/s}^2\text{]} \quad (11)$$

$$d = \frac{2\pi\zeta V}{S\sqrt{1-\zeta^2}}m \qquad \text{[kg/s]} \quad (12)$$

$$h = \frac{\pi^2 V^2}{S\,(1-\zeta^2)}m \qquad \text{[kgm/s}^2\text{]} \quad (13)$$

6 CONCLUSIONS

Overall, nanosecond LIFT was proven with a central wavelength of 1064 nm onto a 400 nm thick gold film:

1. Close matchings of the thermal diffusion length and the laser spot size were found within the morphology of the donor crater. Single droplet depositions in the thin-film regime were found, although glass ablation spots were also found.
2. A threshold laser fluence of 162.48 J/cm^2 was found and lined up with literature for nanosecond LIFT of metals for smaller wavelengths.
3. For the speed range of 20 mm/s to 52 mm/s, a trend of $\delta x_{\hat{\mathbf{v}}} = v \cdot -0.0933$ ms was found.
4. For the acceleration of -1.97 m/s^2 to 1.97 m/s^2, a trend of $\delta x_{\hat{\mathbf{a}}} = a \cdot -0.6085$ ms^2 was found. The observed deviations in translation lined up with literature and were dominant over both trends.
5. For repetition rates between 1 kHz and 10 kHz, no differences in donor morphology were found.
6. A step responses assembly with periodical spacing was created; The next step-input gets excited at the peak time with ejection at the rise time.
7. A valid couple of ζ and the printing speed can be manually chosen with Figure 10. Constraints on the mechanical parameters (m, d, k, h) were found. Equations (11),(12),(13) shows that the coefficients are given by ζ and the printing speed

The results show the viability of the LIFT setup made and can be used for making an experimental LIFT setup, giving constraints on the scalability of LIFT printing speed using a step response assembly and adjusting a system with a changing equivalent mass.
Future research should consist of examining droplet translations for even higher velocities, accelerations, and repetition rates and for different material classes. Additionally, droplet translation in a LIFT setup with a galvanometric scanner and/or carrier-donor and receiver that move independently should be examined.

ACKNOWLEDGEMENTS

This work was supported by the research funding project: "System Analysis meets high-tech applications (SanHTa, UT/VU)". The author wants to express its gratitude to the research chair: "Laser Processing" from the University of Twente, in particular: M.L. Stok - Van Houwelingen, D.E. Sidney, J.J.J. Huaroto Sevilla and C. Herrmann. Additionally, the author wants to express its gratitude to G. Lee and H. Koroglu. The research facilities, materials, and insight provided by all mentioned people have been crucial in the successful completion of this study.

AVAILABILITY OF DATA AND MATERIALS

Supplementary materials are available upon request from s.t.c.fokkema@student.utwente.nl

REFERENCES

During the preparation of this work the author used Writefull in order to improve spelling and general formatting. After using this tool/service, the author reviewed and edited the content as needed and takes full responsibility for the content of the work.

[1] H. I. J. Kals, C. Buiting-Csiós, W. Dewulf, B. Lauwers, J. M. Ponsen, A. H. Streppel, and T. H. J. Vaneker, *Industrial Production: The Manufacture of Mechanical Products*. Boom uitgevers Amsterdam, 2019. sixth edition.

[2] K. Hon, L. Li, and I. Hutchings, "Direct writing technology—advances and developments," *CIRP annals*, vol. 57, no. 2, pp. 601–620, 2008.

[3] P. Serra and A. Piqué, "Laser-induced forward transfer: Fundamentals and applications," *Advanced Materials Technologies*, vol. 4, no. 1, 1800099, 2019.

[4] J. Bohandy, B. Kim, and F. Adrian, "Metal deposition from a supported metal film using an excimer laser," *Journal of Applied Physics*, vol. 60, no. 4, pp. 1538–1539, 1986.

[5] D. A. Willis, "Laser-induced forward transfer of metals," *Laser Printing of Functional Materials: 3D Microfabrication, Electronics and Biomedicine*, pp. 149–174, 2018.

[6] M. P. Giesbers, M. Hoppenbrouwers, E. Smits, and R. Mandamparambil, "Process optimization of lift through visualization: towards high resolution metal circuit printing," in *Laser Sources and Applications II*, vol. 9135, pp. 166–171, SPIE, 2014.

[7] A.-C. Tien, Z. S. Sacks, and F. J. Mayer, "Precision laser metallization," *Microelectronic engineering*, vol. 56, no. 3-4, pp. 273–279, 2001.

[8] A. Narazaki, R. Kurosaki, T. Sato, Y. Kawaguchi, W. Watanabe, and H. Niino, "On-demand preparation of microdot patterns by laser-induced dot transfer," *Journal of Laser Micro Nanoengineering*, vol. 7, no. 1, p. 77, 2012.

[9] C. W. Visser, R. Pohl, C. Sun, G.-W. Römer, and D. Lohse, "Toward 3d printing of pure metals by laser-induced forward transfer," *Advanced materials*, no. 27, pp. 4087–4092, 2015.

[10] M. Feinaeugle, R. Pohl, T. Bor, T. Vaneker, and G. willem Römer, "Printing of complex free-standing microstructures via laser-induced forward transfer (lift) of pure metal thin films," *Additive Manufacturing*, vol. 24, pp. 391–399, 2018.

[11] A. Das, A. Ghosh, S. Chattopadhyaya, and C.-F. Ding, "A review on critical challenges in additive manufacturing via laser-induced forward transfer," *Optics & Laser Technology*, vol. 168, p. 109893, 2024.

[12] D. Wu, G. Luo, Y. Hu, Y. Zhou, and M. Chen, "Printing regime for single metal microdroplet deposition in laser-induced forward transfer," *Optics and Lasers in Engineering*, vol. 167, 107617, 2023.

[13] V. Schultze and M. Wagner, "Blow-off of aluminium films," *Applied Physics A*, vol. 53, pp. 241–248, 1991.

[14] V. Schultze and M. Wagner, "Laser-induced forward transfer of aluminium," *Applied surface science*, vol. 52, no. 4, pp. 303–309, 1991.

[15] I. SPI® Lasers Uk Ltd., "Sm-s00369_d_20w_ep_z_ specification_2016-08-30," 2016. `https://www.spilasers.com/wp-content/uploads/2015/10/20W_EP_Z_specification_2016_08_30_D.pdf`, WFORM 16, last accessed on 30.11.2024.

[16] I. Engineers Edge, "Thermal diffusivity table," `https://www.engineersedge.com/heat_transfer/thermal_diffusivity_table_13953.htm`, last accessed on 30.11.2024.

[17] R. J. Baseman, N. M. Froberg, J. C. Andreshak, and Z. Schlesinger, "Minimum fluence for laser blow-off of thin gold films at 248 and 532 nm," *Applied physics letters*, vol. 56, no. 15, pp. 1412–1414, 1990.

[18] R. Pohl, C. Visser, C. Sun, D. Lohse, *et al.*, "Imaging of the ejection process of nanosecond laser-induced forward transfer of gold," in *15th International Symposium on Laser Precision Microfabrication, LPM 2014*, pp. 129–134, "2014".

[19] I. The Engineering Toolbox, "Boiling points and specific heat of liquid metals.," `https://www.engineeringtoolbox.com/liquid-metal-boiling-points-specific-heat-d_1893.html`, last accessed on 30.11.2024.

[20] P. Pattison, M. Hansen, J. Bardsley, G. Thomson, K. Gordon, A. Wilkerson, K. Lee, V. Nubbe, and S. Donnelly, *2022 Solid-State Lighting R&D Opportunities*. US Department of Energy, Office of Energy Efficiency & Renewable Energy, 2022.

[21] T. Sano, H. Yamada, T. Nakayama, and I. Miyamoto, "Experimental investigation of laser induced forward transfer process of metal thin films," *Applied surface science*, vol. 186, no. 1-4, pp. 221–226, 2002.

[22] V. Rastogi, S. Chaurasia, and D. Munda, "Laser induced damage studies in borosilicate glass using nanosecond and sub nanosecond pulses," *Journal of Non-Crystalline Solids*, vol. 463, pp. 138–147, 2017.

[23] Y.-T. Chen, K.-J. Ma, A. A. Tseng, and P. Chen, "Projection ablation of glass-based single and arrayed microstructures using excimer laser," *Optics & Laser Technology*, vol. 37, no. 4, pp. 271–280, 2005.

[24] D. I. Yakubovsky, A. V. Arsenin, Y. V. Stebunov, D. Y. Fedyanin, and V. S. Volkov, "Optical constants and structural properties of thin gold films," *Optics express*, vol. 25, no. 21, pp. 25574–25587, 2017.

[25] F. Bryant, "Snell's law of refraction," *Physics Bulletin*, vol. 9, no. 12, 317, 1958.

[26] I. Newlight Photonics Inc, "Basic properties of bk7 and n-bk7 glass," `https://www.newlightphotonics.com/BK7-properties.html`, last acesssed on 30.11.2024.

[27] F. E. Udwadia and A. D. Schutte, "Equations of motion for general constrained systems in lagrangian mechanics," *Acta mechanica*, vol. 213, no. 1, pp. 111–129, 2010.

[28] L. Chen, J. Li, and R. Ding, "Identification for the second-order systems based on the step response," *Mathematical and Computer Modelling*, vol. 53, no. 5, pp. 1074–1083, 2011.